EFFICIENT BOX-CONSTRAINED TV-TYPE-l^1 ALGORITHMS FOR RESTORING IMAGES WITH IMPULSE NOISE*

Liyan Ma

School of Computer and Information Technology, Beijing Jiaotong University, Beijing 100044, China
Email: 08112068@bjtu.edu.cn

Michael K. Ng

Department of Mathematics, Hong Kong Baptist University, Hong Kong, China
Email: mng@math.hkbu.edu.hk

Jian Yu

School of Computer and Information Technology, Beijing Jiaotong University, Beijing 100044, China
Email: jianyu@bjtu.edu.cn

Tieyong Zeng

Department of Mathematics, Hong Kong Baptist University, Hong Kong, China
Email: zeng@hkbu.edu.hk

Abstract

In this paper, we study the restoration of images simultaneously corrupted by blur and impulse noise via variational approach with a box constraint on the pixel values of an image. In the literature, the TV-l^1 variational model which contains a total variation (TV) regularization term and an l^1 data-fidelity term, has been proposed and developed. Several numerical methods have been studied and experimental results have shown that these methods lead to very promising results. However, these numerical methods are designed based on approximation or penalty approaches, and do not consider the box constraint. The addition of the box constraint makes the problem more difficult to handle. The main contribution of this paper is to develop numerical algorithms based on the derivation of exact total variation and the use of proximal operators. Both one-phase and two-phase methods are considered, and both TV and nonlocal TV versions are designed. The box constraint $[0, 1]$ on the pixel values of an image can be efficiently handled by the proposed algorithms. The numerical experiments demonstrate that the proposed methods are efficient in computational time and effective in restoring images with impulse noise.

Mathematics subject classification: 65J22, 65K10, 68U10.
Key words: Image restoration, Impulse noise, Total variation, Nonlocal total variation, Proximal Operators.

1. Introduction

In many real applications, the observed image is the degraded version of the true image. Therefore, image restoration is one of the fundamental tasks in image processing, and it plays an important role in many applications. Indeed, image restoration is a typical inverse problem, and many approaches [8, 22, 40, 42, 47] are proposed to tackle this task.

In this paper, we study the restoration of images corrupted by blur and impulse noise simultaneously via the variational approach with a box constraint on the pixel values of an

image. Note that usually image blur comes from many facts such as camera shaking, object movement or an out of focus lens. Moreover, impulse noise is often found and modeled in digital storage and transmission. Since each image pixel stands for light intensity whose value is nonnegative and finite, one would like to recover the image with pixel values in the same range. In this paper, we assume that the values of the all pixels of the images are in the range $[0, 1]$ for simplicity. The importance of box constraints was emphasized by [26, 31, 35, 41] and references therein.

Assume that both the true image u and the corrupted image g are defined on $\Omega \subseteq \mathbb{R}^{m \times n}$, the image degradation model can be written as follows:

$$g = N_{imp}(Au), \tag{1.1}$$

where A is a known linear operator from $\mathbb{R}^{m \times n}$ to $\mathbb{R}^{m \times n}$, N_{imp} represents the degradation by the impulse noise.

In the literature, there are two common types of impulse noise: salt-and-pepper noise and random-valued noise [10, 11, 46]. Suppose that the noise level is r ($0 \leq r \leq 1$), the model of corruption by the salt-and-pepper noise at location (i, j) can be defined as:

$$g_{ij} = \begin{cases} 0, & \text{with probability } r/2, \\ 1, & \text{with probability } r/2, \\ (Au)_{ij}, & \text{with probability } 1 - r, \end{cases}$$

and the model of corruption by the random-valued noise at location (i, j) is:

$$g_{ij} = \begin{cases} d_{ij}, & \text{with probability } r, \\ (Au)_{ij}, & \text{with probability } 1 - r, \end{cases} \tag{1.2}$$

where the values $d_{ij} \in [0, 1]$ come from an independent and identically distributed uniform random numbers in $[0, 1]$. One can obviously observe that both salt-and-pepper noise and the random-valued noise corrupt a certain number of image pixels and keeps the remaining pixels uncorrupted. As the value $d_{i,j}$ in (1.2) poses another uncertainty, one can understand that the random-valued noise is more difficult to handle than the salt-and-pepper noise (see [46]).

In the past, various approaches have been proposed for removing the impulse noise. One is the filtering technique, and the most popular filter is the median filter [39] which is efficient and easy to be implemented. However, the median filter often makes the recovered image blurry because it accomplishes the filtering task via replacing each pixel in the image by the median value in a window centered on it. Thus, some modified versions of the median filter are proposed, such as the weighted median filter [7], the adaptive median filter [28], the multi-state median filter [12], the center-weighted median filter [32], etc. Although these modified filters can preserve more details in the recovered image than the median filter, they still cannot preserve the image edges well especially when the noise level is high.

Recently, by combing an l^1 data-fidelity term and an edge-preserving regularization term, Nikolova [38] proposed a method to better preserve the edge information based on the variational approach. It is shown that the l^1 data-fidelity term has rather good performance on detecting outlier and removing impulse noise [37, 38]. However, this method changes the values of the uncorrupted pixels. Based on the self-similarity of natural images [16], Xiao et al. [46] proposed a powerful patch-based method to remove mixed Gaussian-impulse noise. They obtain much better results than the compared methods.

In the above methods, the blurry of the corrupted images has not been considered. Indeed the blurry is almost not avoidable in the acquisition of the images, and many existing methods aim to recover the images which are corrupted by blur and impulse noise. Bar et al. [2, 3] proposed a model which is composed of the Mumford-Shah regularizer and the l^1-like data-fidelity term to deblur the image and remove the impulse noise. Later, Bar et al. [4] generalized this model to color image deblurring under impulse noise. Furthermore, Cai et al. [10] proposed a two-phase method which yields much better results than the traditional one-phase methods. In the first phase, they use the median-type filter to identify the corrupted pixels. In the second phase, the data-fidelity term of the model only utilizes the uncorrupted pixels to recover the corrupted image. However, due to the problem of the Mumford-Shah regularizer [36], the above models are non-convex and there may exist many local minima.

Since the TV regularization is convex and can preserve sharp edges, the TV-l^1 model is widely applied to image deblurring under impulse noise. However, it is difficult to solve the TV-l^1 model due to the non-differentiability of the norm. Recently, by introducing two auxiliary variables, Yang et al. [48] proposed an efficient algorithm (FTVd) for solving the TV-l^1 model and explained that the quadratic penalty method [43] applied to properly split problems is equivalent to Huber-type regularization. Similarly, Guo et al. [23] employed an alternating minimization method to restore blurred and noisy images. Dong et al. [21] investigated this model via a primal-dual approach, and in their model, the data-fidelity term and the regularization term are Huber-type functionals. To reduce the computational cost, Wu et al. [45] introduced the augmented Lagrangian method to solve this model at the cost of the lower restored quality. Later, Chan et al. [15] extended the work [21] to get a two-phase method. Recently, Cai et al. [11] minimized a TV-l^1-like model by a fixed-point method, then used the preconditioned conjugate method to solve the resulting inner linear systems.

Experimental results have shown that the above mentioned numerical methods lead to very promising results. However, these numerical methods are designed based on approximation or penalty approaches. And few papers focus on constrained TV-type-l^1 problems. The main contribution of this paper is to develop numerical algorithms based on the derivation of exact total variation and the use of proximal operators for constrained TV-type-l^1 models. In our approach, the computation of the inverse of the term $A^{\mathrm{T}}A$ is avoided, and it is not necessary to solve inner iterations that are required in [11, 23, 48]. Also the proposed approach can handle efficiently the box constraint $[0, 1]$ on the pixel values of an image. Moreover, both one-phase and two-phase methods are considered, and both TV and nonlocal TV versions are designed. The convergence of these numerical methods will be shown. The experimental results demonstrate that the proposed methods are efficient in computational time and effective in restoring images with impulse noise.

The outline of this paper is given as follows. In Section 2, we give some notations and preliminaries which will be used in the paper. In Section 3, we introduce the proposed algorithms. Precisely, we first present a general constrained model and the algorithm to solve this model; and then we specific how to use this general constrained model as one-phase method and two-phase method for image deblurring with impulse noise. In Section 4, numerical results are reported to demonstrate the good performance of the proposed algorithms. In Section 5, we give the conclusion of the paper.

2. Notations and Preliminaries

2.1. Notations

Throughout the paper, let X be a real vector space $\mathbb{R}^{m \times n}$. Denote the discrete image as $u \in X$, written as an $m \times n$ matrix. Let $\langle \cdot, \cdot \rangle$ denote the standard inner product, and $\|\cdot\|_p$ be the standard l^p-norm. Let A be a linear transform, and its complex conjugate transpose A^* is characterized by $\langle Au, g \rangle = \langle u, A^*g \rangle$ for all u, g. Let us denote I as the identity matrix.

For any set $A \subseteq \mathbb{R}^n$, the indicator function δ_A is defined by:

$$\delta_A(x) = \begin{cases} 0, & \text{if} \quad x \in A, \\ +\infty, & \text{otherwise,} \end{cases}$$

and the characteristic function χ_A is given by:

$$\chi_A(x) = \begin{cases} 1, & \text{if } x \in A, \\ 0, & \text{otherwise.} \end{cases}$$

2.2. The discrete gradient and divergence operators

In this paper, the periodic boundary conditions are adopted to define discrete gradient and divergence operators since the DFT will be used to compute the convolution operator. Precisely, the discrete operators ∂_x, ∂_y are defined as:

$$(\partial_x u)_{i,j} = \begin{cases} u_{i+1,j} - u_{i,j}, & \text{if} \quad 1 \leq i < m, \\ u_{1,j} - u_{i,j}, & \text{if} \quad i = m, \end{cases}$$

and

$$(\partial_y u)_{i,j} = \begin{cases} u_{i,j+1} - u_{i,j}, & \text{if} \quad 1 \leq j < n, \\ u_{i,1} - u_{i,j}, & \text{if} \quad j = n. \end{cases}$$

The discrete operators ∂_x^* and ∂_y^* are defined as:

$$(\partial_x^* p)_{i,j} = \begin{cases} p_{i,j} - p_{m,j}, & \text{if} \quad i = 1, \\ p_{i,j} - p_{i-1,j}, & \text{if} \quad 1 < i \leq m, \end{cases}$$

and

$$(\partial_y^* q)_{i,j} = \begin{cases} q_{i,j} - q_{i,n}, & \text{if} \quad j = 1, \\ q_{i,j} - q_{i,j-1}, & \text{if} \quad 1 < j \leq m. \end{cases}$$

Denote $U = \mathbb{R}^{m \times n} \times \mathbb{R}^{m \times n}$. The gradient operator is a map $\nabla : \mathbb{R}^{m \times n} \to U$ which is defined as $\nabla u = (\partial_x u, \partial_y u)^{\mathrm{T}}$. For $z = [p, q]^{\mathrm{T}} \in U$, the divergence operator div is defined as:

$$\text{div}(u) = -\nabla^* u = -(\partial_x^* p + \partial_y^* q).$$

The maximum norm of $z \in U$ is given as

$$\|z\|_\infty := \max_{i,j} \left| \sqrt{p_{i,j}^2 + q_{i,j}^2} \right|. \tag{2.1}$$

2.3. Primal-dual approach

Recently, many methods [13, 17, 21, 50] have been proposed and studied for solving convex optimization problems via the dual or the primal-dual approach. The main reason is that they are more efficient than the primal approach in image processing when solving non-differentiable convex optimization problems arising in total variation regularization.

Note that the non-differentiable convex optimization problems also can be solved by other efficient methods, such as augmented Lagrange method [45] and the split Bregman method [25]. However, the two methods do not exactly solve the non-differentiable convex optimization problems. Thus in this paper, we adopt the primal-dual framework, and we briefly review it as follows.

Let $F : X \to [0, +\infty)$ and $G : X \to [0, +\infty)$ be proper, convex, lower semi-continuous functions. The following primal minimization problem is considered:

$$\min_u F(Ku) + G(u), \tag{2.2}$$

where $K : X \to Y$ (Y be another real vector space) is a linear map with the following norm:

$$\|K\|_2 = \max \left\{ \|Ku\|_2 : u \in X \quad \text{with } \|u\|_2 \leq 1 \right\}.$$

The convex conjugate F^* of F [5] is given by:

$$F^*(p) = \sup_w \langle p, w \rangle - F(w).$$

Since $F^{**} = F$, we have:

$$F(Ku) = \sup_{p \in Y} \langle p, Ku \rangle - F^*(p).$$

Thus the primal-dual formulation of (2.2) can be written as follows:

$$\min_{u \in X} \max_{p \in Y} \langle Ku, p \rangle + G(u) - F^*(p). \tag{2.3}$$

Note that the dual problem of (2.3) is:

$$\max_{p \in Y} F_d(p), \tag{2.4}$$

where $F_d(p) = \min_{u \in X} \langle Ku, p \rangle + G(u) - F^*(p)$.

2.4. Proximal operators

Moreau [33, 34] first introduced the concept of proximal operators which have been widely used in convex optimization [14, 19]. For a continuous proper, convex and lower semi-continuous function φ on $\mathbb{R}^{m \times n}$, its proximal operator is defined as follows:

$$\mathrm{prox}_\varphi(x) = \arg\min_y \varphi(y) + \frac{1}{2} \|x - y\|_2^2.$$

Obviously, this model is strictly convex. Thus, there exists a unique point $\mathrm{prox}_\varphi(x)$, and prox_φ can be easily computed.

3. The Proposed Constrained Model

Recently, Chambolle and Pock [14], and Werlberger et al. [44] have studied the primal-dual formulation of the TV-l^1 model for video interpolation and restoration. Inspired by their works, in this section, we consider the box-constrained TV-type-l^1 model for image deblurring under impulse noise. We present the general form of the proposed methods in this section. Then we give the specific form of the one-phase and two-phase methods for image deblurring under impulse noise in next section.

Recall that we set X as $\mathbb{R}^{m \times n}$. The general formulation considered in this paper for image deblurring under impulse noise is given as follows:

$$\min_{0 \leq u \leq 1} \|f_1(u)\|_1 + \lambda \|f_2(Au - g)\|_1, \tag{3.1}$$

where f_1 is linear operator from X to $X \times X$, and f_2 is linear operator from X to itself. The first term is the TV-type regularization and f_1 is often taken as the gradient operator or non-local gradient operator (see below); the second term is the l^1 data-fidelity term which measures the distance between the recovered image and the observed one, and typically f_2 is the identity operator. We specific the choice of f_1, f_2 for our image deblurring task under impulse noise in the coming subsection. Again, A is the linear convolution operator from X to itself, and $\lambda > 0$ is a balance parameter. Note that comparing with the previous works [10, 11, 14, 37, 38, 48], our model here is rather new since we consider the box constraint $0 \leq u \leq 1$, which is physically reasonable and useful.

3.1. Primal-dual formulation

Since the primal-dual approach is more efficient than the primal approach when solving non-differentiable convex optimization problems, we rewrite (3.1) into its primal-dual formulation. Indeed, this is not too difficult. Let us set:

$$P \quad := \quad \{p \in X \times X, \|p\|_\infty \leq 1\}, \tag{3.2}$$

$$Q \quad := \quad \{q \in X, \|q\|_\infty \leq \lambda\}, \tag{3.3}$$

$$S \quad := \quad \{u \in X, 0 \leq u \leq 1\}, \tag{3.4}$$

and assume that δ_P, δ_Q and δ_S are the indicator functions correspondingly. By introducing two dual variables, we have:

Proposition 3.1. *The* (3.1) *is equivalent to the following min-max problem:*

$$\max_{(p,q) \in Y} \min_{u \in X} \langle f_1(u), p \rangle + \langle f_2(Au - g), q \rangle - \delta_P(p) - \delta_Q(q) + \delta_S(u), \tag{3.5}$$

where Y is the space where (p, q) lives, or precisely, it is $(X \times X) \times X$.

Proof. As we known, the dual norm of $\|\cdot\|_1$ is $\|\cdot\|_\infty$ [5]. Thus the conjugate of $F(x) = \lambda \|x\|_1$ is :

$$F^*(y) = \begin{cases} 0, & \|y\|_\infty \leq \lambda, \\ \infty, & \text{otherwise.} \end{cases}$$

Hence, based on the knowledge of the primal-dual approach introduced in Section 2.3, we can rewrite (3.1) as:

$$\max_{(p,q) \in Y} \min_{u \in S} \langle f_1(u), p \rangle + \langle f_2(Au - g), q \rangle - \delta_P(p) - \delta_Q(q). \tag{3.6}$$

Since (3.6) is convex and S is a convex set, then this constrained problem has the same minimizer with the unconstrained problem (3.5) [27]. Then the (3.1) is equivalent to the min-max problem (3.5).   □

The formulation (3.5) is an extension of the approach given in [14, 37, 38]. Based on the above general formulation, both one-phase and two-phase methods will be considered, and both TV and nonlocal TV versions can be designed, see section below.

Proposition 3.2. *The saddle point set of* (3.5) *is nonempty.*

Proof. We remark that we can easily verify that the required conditions in [27]:

- (H1): X and Y are nonempty closed convex sets;

- (H2): ℓ (denote the objective function in (3.5)) is convex-concave on $X \times Y$ in the following sense: for each $y \in Y$, the function $\ell(\cdot, y)$ is convex, for each $x \in X$, the function $\ell(x, \cdot)$ is concave;

- (H3): X is bounded, or there exists $y_0 \in Y$ such that $\ell(x, y_0) \to +\infty$ when $\|x\| \to +\infty$;

- (H4): Y is bounded, or there exists $x_0 \in X$ such that $\ell(x_0, y) \to +\infty$ when $\|y\| \to +\infty$;

are satisfied for the proposed primal-dual formulation.   □

Thus, there exists a nonempty convex compact set of saddle-points on $X \times Y$ for each version: one-phase, two-phase, TV and nonlocal TV (for details, see (4.1), (4.4), (4.7) below). Now let us address the algorithm to solve the general model.

3.2. Algorithm for the general model

Recently, many primal-dual algorithms [14,21,50] are proposed. Here, inspired by Chambolle and Pock [14], and based on the derivation of exact total variation in the above primal-dual formulation, we can make use of proximal operators to optimize (3.5), and develop the following algorithm:

$$
\begin{cases}
p^{n+1} = \text{Prox}_{\delta_P}\left(p^n + t_d f_1(\bar{u})\right), \\
q^{n+1} = \text{Prox}_{\delta_Q}\left(q^n + t_d f_2(\bar{u})\right), \\
u^{n+1} = \text{Prox}_{\delta_S}\left(u^n - t_u \partial_u \left(\left\langle f_1(u^n), p^{n+1}\right\rangle + \left\langle f_2(Au^n - g), q^{n+1}\right\rangle\right)\right), \\
\bar{u} = 2u^{n+1} - u^n,
\end{cases}
\tag{3.7}
$$

where t_d and t_u are the time steps. More precisely, the above proximal operators are given by:

$$
\begin{aligned}
\text{Prox}_{\delta_P}(p) &= \frac{p}{\max(1, |p|)}, \\
\text{Prox}_{\delta_Q}(q) &= \frac{\lambda q}{\max(\lambda, |q|)}, \\
\text{Prox}_{\delta_S}(u) &= \max\left(\min\left(u, 1\right), 0\right).
\end{aligned}
\tag{3.8}
$$

Comparing (3.7) with the Algorithm 1 in [14], we can see that the proposed algorithm is an extension of the Algorithm 1 in [14] to deal with deblurring under impulse noise. Indeed, denote $y = (p, q)$, and assume that $K = \left(\begin{array}{cc} f_1^{\text{T}} & (f_2 A)^{\text{T}} \end{array}\right)^{\text{T}}$, then the min-max problem (3.6) can be rewritten as:

$$
\max_y \min_u \langle Ku, y \rangle + G(u) - F^*(y),
$$

where $G(u) = \delta_S(u)$, and $F^*(y) = \delta_P(p) + \delta_Q(q) + \langle f_2(g), q \rangle$. As both G and F^* are proper, convex, l.s.c functions, this is exactly the same problem studied in [14], see (2) there or (2.3). In other words, as the data-fidelity term takes l^1 norm in this paper, we introduce an extra dual variable to rewrite this term to its dual formulation. Thus we can exactly solve the minimization problem (3.1) by (3.7).

The convergence of the above proposed algorithm can be guaranteed by the following theorem if the time steps t_d, t_u are small enough.

Theorem 3.1. *Let $L = \|K\|_2$, where $K = \left(\begin{matrix} f_1^{\mathrm{T}} & (f_2 A)^{\mathrm{T}} \end{matrix} \right)^{\mathrm{T}}$. Choose $t_d t_u L^2 < 1$, and let $\{u^n\}$, $\{p^n\}$ and $\{q^n\}$ be generated by the algorithm (3.7). Let*

$$u_N = \frac{1}{N} \sum_{n=1}^{N} u^n, \quad p_N = \frac{1}{N} \sum_{n=1}^{N} p^n, \quad q_N = \frac{1}{N} \sum_{n=1}^{N} q^n,$$

and the partial primal-dual gap be:

$$Gap\,(u, p, q) = \max_{p'} \ell\,(u, p', q) + \max_{q'} \ell\,(u, p, q') - \min_{u'} \ell\,(u', p, q).$$

Then there exists a constant $C > 0$ such that

$$Gap\,(u_N, p_N, q_N) \leq \frac{C}{N}. \tag{3.9}$$

One can easily prove this theorem following the proof of Theorem 1 in [14].

According to (3.7), we can observe that the proposed primal-dual algorithm is very simple and easy to be implemented. In the approach, the computation of the inverse of the term $A^{\mathrm{T}} A$ is avoided, and it is not necessary to solve inner iterations that are required in [11, 23, 48]. Also the proposed approach can efficiently handle the box constraint $[0, 1]$ on the pixel values of an image.

Note that, recently, Dong [20] studied the TV-l^1 model by introducing a tight frame based regularization for image deblurring and impulse noise removal. They used the split Bregman algorithm to solve the corresponding model. We can also use the proposed algorithm to solve this model. However, we find it is time consuming to compute the tight frame coefficients at each iteration, and the experimental results are not better than those given by the proposed pdNLTV2 algorithm. Thus we will not consider the tight frame based regularization in the following discussion.

4. The One-Phase and Two-Phase Methods

In this section, we first give the specific form of the one-phase model which contains a TV regularization and an l^1 data-fidelity term. Since the two phase method is more effective for image deblurring under impulse noise, we then introduce the specific form of the two-phase method.

Since the nonlocal TV regularization needs to calculate the nonlocal similarity of the image patches, and it is not suitable to compute the similarity based on the corrupted image, thus we only use the nonlocal TV regularization in the two-phase method, and use the filtered image to calculate the nonlocal similarity.

4.1. One-phase method

In this subsection, we will give the specific formulation form (3.7) for the one-phase method of the TV regularization. The constrained TV-l^1 model for image deblurring under impulse noise is defined by:

$$\min_{0 \le u \le 1} \|\nabla u\|_1 + \lambda \|Au - g\|_1. \tag{4.1}$$

Comparing (4.1) with (3.1), here, we have $f_1 = \nabla$ and $f_2 = I$.

Notice that classically, we have:

$$\|\nabla u\|_1 = \max_{\|p\|_\infty \le 1} \langle \nabla u, p \rangle,$$

where $\|p\|_\infty$ is defined in (2.1). Moreover, the primal-dual formulation of (4.1) can be written as:

$$\max_{p,q} \min_u - \langle u, \operatorname{div} p \rangle + \langle Au - g, q \rangle - \delta_P(p) - \delta_Q(q) + \delta_S(u), \tag{4.2}$$

where again we have set P, Q, S in (3.2)-(3.4). Moreover, δ_P, δ_Q and δ_S is the indicator function correspondingly.

Following (3.7), the algorithm (named pdTV1) for solving (4.2) is given by:

$$\begin{cases} p^{n+1} = \operatorname{Prox}_{\delta_P}\left(p^n + t_d \nabla \bar{u}\right), \\ q^{n+1} = \operatorname{Prox}_{\delta_Q}\left(q^n + t_d\left(A\bar{u} - g\right)\right), \\ u^{n+1} = \operatorname{Prox}_{\delta_S}\left(u^n - t_u\left(-\operatorname{div} p^{n+1} + A^* q^{n+1}\right)\right), \\ \bar{u} = 2u^{n+1} - u^n, \end{cases} \tag{4.3}$$

where the proximal operators can be computed by (3.8) efficiently.

Here, we have

$$L \le \sqrt{\|\nabla\|_2^2 + \|A\|_2^2}.$$

Since $\|\nabla\|_2^2 \le 8$ (see [13]), then we have $L^2 \le 9$ if $\|A\|_2$ is small. Note that in the continuous settings, usually $Au = k * u$, where the point spread function k satisfies:

$$k \ge 0, \quad \int_{\mathbb{R}^2} k(x)dx = 1.$$

Thus by Lemma 1.4 of [1], for any $u \in L^2(\mathbb{R}^2)$, we have: $\|Au\|_2 = \|k * u\|_2 \le \|k\|_1 \|u\|_2 = \|u\|_2$. Hence, roughly we can assume that: $\|A\|_2 \le 1$.

4.2. Two-phase method

In this subsection, we consider the two-phase method which can achieve much better results than the one-phase methods. This is because that the two-phase methods utilize the characteristic of impulse noise: some pixels are noise-free. Thus the first step of the two-phase method is to detect the noise candidate pixels. Here, we use two simple filters to detect the salt-and-pepper noise and the random-valued noise, named the adaptive median filter (AMF) [28] and the adaptive center-weighted median filter (ACWMF) [32] respectively.

Let z be the filtered image obtained from applying AMF or ACWMF on the corrupted image g, which is defined on the grid Ω. Let Ω_N be the set of noise candidate pixels. Then Ω_N can be obtained by:

- For the salt-and-pepper noise:

$$\Omega_N = \{(i,j) \in \Omega : z_{ij} \neq g_{ij} \text{ and } z_{ij} \in \{0,1\}\},$$

- For the random-valued noise:

$$\Omega_N = \{(i,j) \in \Omega : z_{ij} \neq g_{ij}\}.$$

We only use the detected uncorrupted pixels in the data-fidelity term. Although there exist errors in the detection (the error is even larger when the image is corrupted by the random-valued noise), the experimental results in Section 4 show that the first step detection is very useful and the two-phase methods can obtain better performance in image restoration than the one-phase methods. Next, we present two algorithms based on TV regularization and nonlocal TV regularization respectively.

4.2.1. Constrained TV-l^1

With the information obtained from applying the median-type filtering on the corrupted images, the formulation of the constrained TV-l^1 model for the two-phase method can be defined as:

$$\min_{0 \leq u \leq 1} \|\nabla u\|_1 + \lambda \left\| \chi_{\Omega \backslash \Omega_N} \left(Au - g \right) \right\|_1. \tag{4.4}$$

Similarly, after introducing two dual variable, we rewrite (4.4) to its primal-dual formulation:

$$\max_{p,q} \min_u - \langle u, \operatorname{div} p \rangle + \left\langle \chi_{\Omega \backslash \Omega_N} \left(Au - g \right), q \right\rangle - \delta_P(p) - \delta_Q(q) + \delta_S(u). \tag{4.5}$$

Then the algorithm (named pdTV2) for solving (4.5) is given as follows:

$$\begin{cases} p^{n+1} = \operatorname{Prox}_{\delta_P} \left(p^n + t_d \nabla \bar{u} \right), \\ q^{n+1} = \operatorname{Prox}_{\delta_Q} \left(q^n + t_d \chi_{\Omega \backslash \Omega_N} \left(A\bar{u} - g \right) \right), \\ u^{n+1} = \operatorname{Prox}_{\delta_S} \left(u^n - t_u \left(-\operatorname{div} p^{n+1} + A^* \chi_{\Omega \backslash \Omega_N} q^{n+1} \right) \right), \\ \bar{u} = 2u^{n+1} - u^n, \end{cases} \tag{4.6}$$

where the proximal operators can be computed by (3.8).

Here,

$$L \leq \sqrt{\|\nabla\|_2^2 + \left\| \chi_{\Omega \backslash \Omega_N} A \right\|_2^2},$$

then we have $L^2 \leq 9$ if $\|\chi_{\Omega \backslash \Omega_N} A\|_2$ is small.

4.2.2. Constrained nonlocal TV-l^1

In this subsection, we consider nonlocal TV (NLTV) as the regularization term. It is well-known that the images are self-similar [16], and many works reach better visual quality by exploiting nonlocal similarity of the image patches than those which just exploit the similarity between pixels.

Buades et al. [8, 9] proposed the famous nonlocal means algorithm for denoising, and it can restore much textures of the noisy image. Later, from the variational view, Gilboa and Osher [24] defined the NLTV regularization for iterative diffusion process, and Zhang et al. [49] applied this regularization to the image deconvolution and sparse reconstruction. Jung et

al. [29,30] proposed the nonlocal Mumford-Shah regularizer which introduces more parameters. Here, we use the NLTV regularization to deblur images with impulse noise.

We use the definitions of the non-local functionals presented in [6,24]. Recall that Ω is the grid where the image lives. For each image u, the nonlocal gradient $\nabla_w u$ maps a pair of pixels $(x, y) \in \Omega \times \Omega$ to a real number:

$$(\nabla_w u)(x, y) = (u(y) - u(x))\sqrt{w(x, y)}, \quad \forall x, y \in \Omega,$$

where w is the edge weight between the pixels located at x and y, and w can be defined as follows:

$$w(u, h)(x, y) = e^{\left\{-\int_\Omega G_a * \|g(x+z) - g(y+z)\|_2^2 dz / h^2\right\}},$$

where $\int_\Omega G_a * \|g(x+z) - g(y+z)\|_2^2 \, dz$ is the distance between patches at the location x and y of the given corrupted image g, G_a is a Gaussian function with standard deviation a and h is a filtering parameter which is dependent on the noise level. According to the above definition, w is symmetric.

Then the NLTV regularization is defined as:

$$\min_u \|\nabla_w u\|_1,$$

where $|\nabla_w u|(x) = \sqrt{\int_\Omega (u(y) - u(x))^2 w(x, y) \, dy}$.

With the noise candidates information, the constrained NLTV-l^1 model for image deblurring under impulse noise can be defined as:

$$\min_{0 \leq u \leq 1} \|\nabla_w u\|_1 + \lambda \|\chi_{\Omega \backslash \Omega_N}(Au - g)\|_1. \tag{4.7}$$

As the definitions in [6,24], the divergence of the dual variable p can be computed by:

$$(\operatorname{div}_w p)(x) = \int_\Omega (p(x, y) - p(y, x))\sqrt{w(x, y)} dy,$$

and we have

$$\langle \nabla_w u, p \rangle = -\langle u, \operatorname{div}_w p \rangle.$$

Then the primal-dual formulation of (4.7) is:

$$\max_{p,q} \min_u -\langle u, \operatorname{div}_w p \rangle + \langle \chi_{\Omega \backslash \Omega_N}(Au - g), q \rangle - \delta_P(p) - \delta_Q(q) + \delta_S(u). \tag{4.8}$$

Thus the two-phase algorithm (named pdNLTV2) for solving (4.7) is given as follows:

$$\begin{cases} p^{n+1} = \operatorname{Prox}_{\delta_P}(p^n + t_d \nabla_w \bar{u}), \\ q^{n+1} = \operatorname{Prox}_{\delta_Q}(q^n + t_d \chi_{\Omega \backslash \Omega_N}(A\bar{u} - g)), \\ u^{n+1} = \operatorname{Prox}_{\delta_S}(u^n - t_u(-\operatorname{div}_w p^{n+1} + A^* \chi_{\Omega \backslash \Omega_N} q^{n+1})), \\ \bar{u} = 2u^{n+1} - u^n, \end{cases} \tag{4.9}$$

where again, the proximal operators can be computed by (3.8) efficiently.

Here,

$$L \leq \sqrt{\|\nabla_w\|_2^2 + \|\chi_{\Omega \backslash \Omega_N} A\|_2^2}.$$

Since $\|\nabla_w\|_2^2 \leq 4N_n$ (N_n is the maximal number of the neighbors of a pixel) (see [24]) and usually $\|\chi_{\Omega \backslash \Omega_N} A\|_2 \leq 1$, then we have $L^2 \leq 4N_n + 1$. However, in practice, the optimal L^2 sometimes may take smaller value for this algorithm. The same problem appeared in [13].

In the next section, we will show that the proposed algorithms are efficient in computational time and effective in restoring images with impulse noise.

5. Experimental Results

In this section, we illustrate the performance of the proposed algorithms and compare it to the FTVd algorithm [48], the ALM algorithm, the algorithm (denoted by Cai2008) in [10] and the algorithm (denoted by Cai2010) in [11]. To compute the weights in the NLTV regularization, the code provided by Bresson [1] is used. We use the 256×256 Cameraman image for example, and only give numerical results of the restoration of other images in Section 5.3. All the images are blurred by a 7×7 Gaussian blur with standard deviation 5 (generated by the MATLAB function 'fspecial').

The compared four algorithms are unconstrained algorithms. However, some of them use the box constraint as the post-processing step to project the all pixel values back to [0, 1]. In this paper, we do this post-processing for the four algorithms, and this enable us to get slightly better results for each algorithm.

The experiments were performed under Windows Vista Premium and MATLAB R2011a running on a laptop with an Intel Core 2 Duo 2.70 GHz.

The signal-to-noise ratio (SNR) is adopted to measure the quality of the restored images. It is defined by:

$$\text{SNR}(u, \tilde{u}) = 10 * \log_{10} \frac{\|\tilde{u} - E(\tilde{u})\|_2^2}{\|\tilde{u} - u\|_2^2},$$

where u denotes the restored image, $\tilde{u}$ denotes the original image and $E(\tilde{u})$ is the mean intensity value of $\tilde{u}$. The stopping criterion is the relative difference between the successive iterates of the restored image (RDS) which is commonly used [11, 14, 48], and is defined by:

$$RDS\left(u^{n+1}, u^n\right) = \frac{\left\|u^{n+1} - u^n\right\|_2}{\left\|u^{n+1}\right\|_2}.$$

We stop all the algorithms whenever $RDS\left(u^{n+1}, u^n\right) < \varepsilon$ (here ε is a small positive constant which means that the results of the algorithms change little) except for the ALM algorithm where we use the stopping criterion as suggested in [45].

In order to get fast convergence and high SNR, we set $t_d t_u = 1/8$ for the algorithms pdTV1, pdTV2 and pdNLTV2 except for the experiments on the images blurred and corrupted by the salt-and-pepper noise with noise levels 30%, 40%, 50%, 60% we set $t_d t_u = 1$ for pdNLTV2.

Table 5.1: SNR (dB) and computational times (in seconds) for the one-phase methods for the corrupted Cameraman image.

	salt-and-pepper				random-valued				
	30%	40%	50%	60%	20%	30%	40%	50%	Average
FTVd	14.69	13.56	12.65	11.38	17.32	13.90	12.69	10.45	13.33
	(18.4s)	(18.3s)	(19.0s)	(19.2s)	(18.8s)	(17.6s)	(17.7s)	(18.1s)	(18.4s)
ALM	14.28	13.19	12.35	11.07	16.68	13.49	12.45	10.38	12.99
	(5.2s)	(4.4s)	(5.0s)	(5.7s)	(6.5s)	(3.7s)	(4.4s)	(2.8s)	(4.7s)
pdTV1	14.72	13.60	12.67	11.37	17.33	13.93	12.73	10.61	13.37
	(6.6s)	(5.8s)	(5.4s)	(4.9s)	(8.4s)	(5.7s)	(4.9s)	(4.6s)	(5.8s)

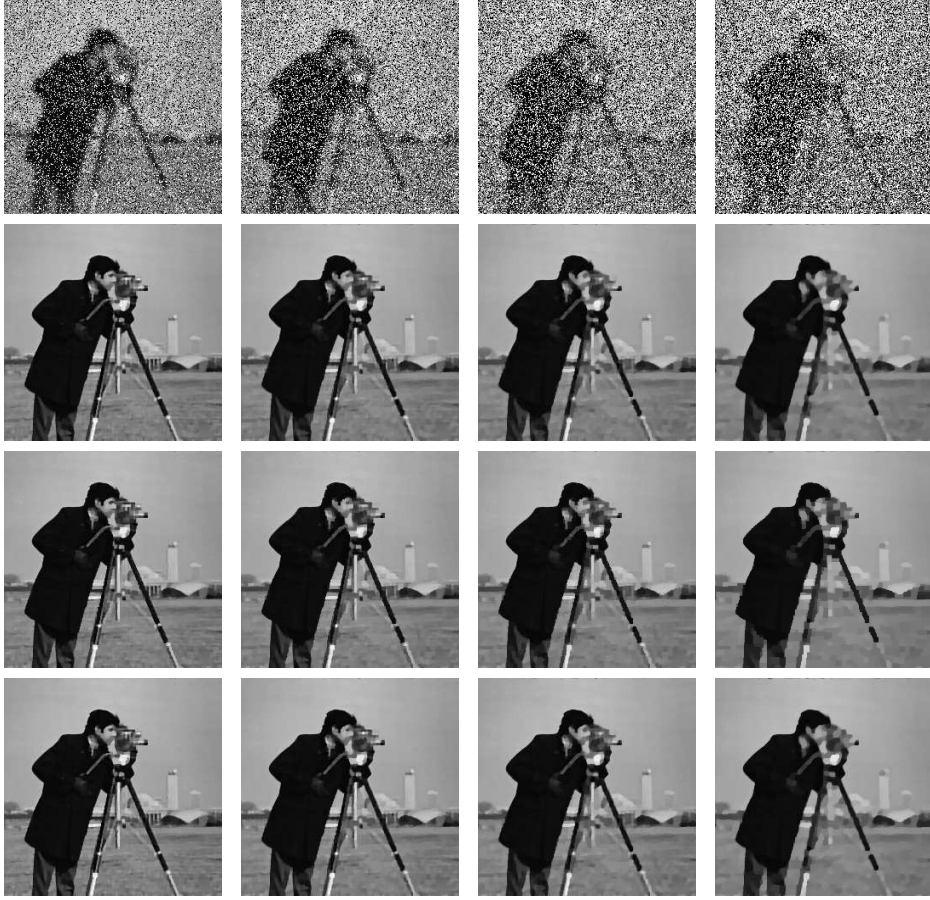[1] http://www.cs.cityu.edu.hk/ xbresson/ucla/code.html

Fig. 5.1. One-phase methods for restoration of the corrupted Cameraman images. The first row is the images corrupted by blur and the salt-and-pepper noise with noise levels 30%, 40%, 50% and 60% respectively. The rest rows from top to bottom give the images recovered by FTVd, ALM and proposed pdTV1.

5.1. One-phase method

In this subsection, we give the experiments on the Cameraman image blurred and corrupted by the salt-and-pepper noise with noise levels 30%, 40%, 50%, 60%, corrupted by random-valued noise with noise levels 20%, 30%, 40%, 50% respectively. We use the same values for λ for all algorithms in this subsection at the same noise level as suggested in [48], and for the salt-and-pepper noise, $\lambda = 13, 10, 8, 4$ respectively, for the random-valued noise, $\lambda = 25, 10, 8, 4$ respectively.

When implementing the FTVd method, we use the the toolbox FTVd 2.0 downloaded from the authors' website. For the algorithm ALM, as suggested in [45], the parameters (r_p, r_z) are set to be (20, 100), (20, 100), (10, 100), (10, 25) for the different levels of the salt-and-pepper noise respectively, and (20, 150), (50, 100), (10, 150), (50, 50) for the different levels of the random-valued noise respectively. For the proposed algorithm pdTV1, we set $t_u = 0.07/\lambda$ for the salt-and-pepper noise and $t_u = 0.06/\lambda$ for the random-valued noise.

The restored images are shown in Fig. 5.1 and Fig. 5.2. The comparisons are given in Table 5.1. One can clearly observe that the resulting SNRs of the ALM algorithm are the lowest, the
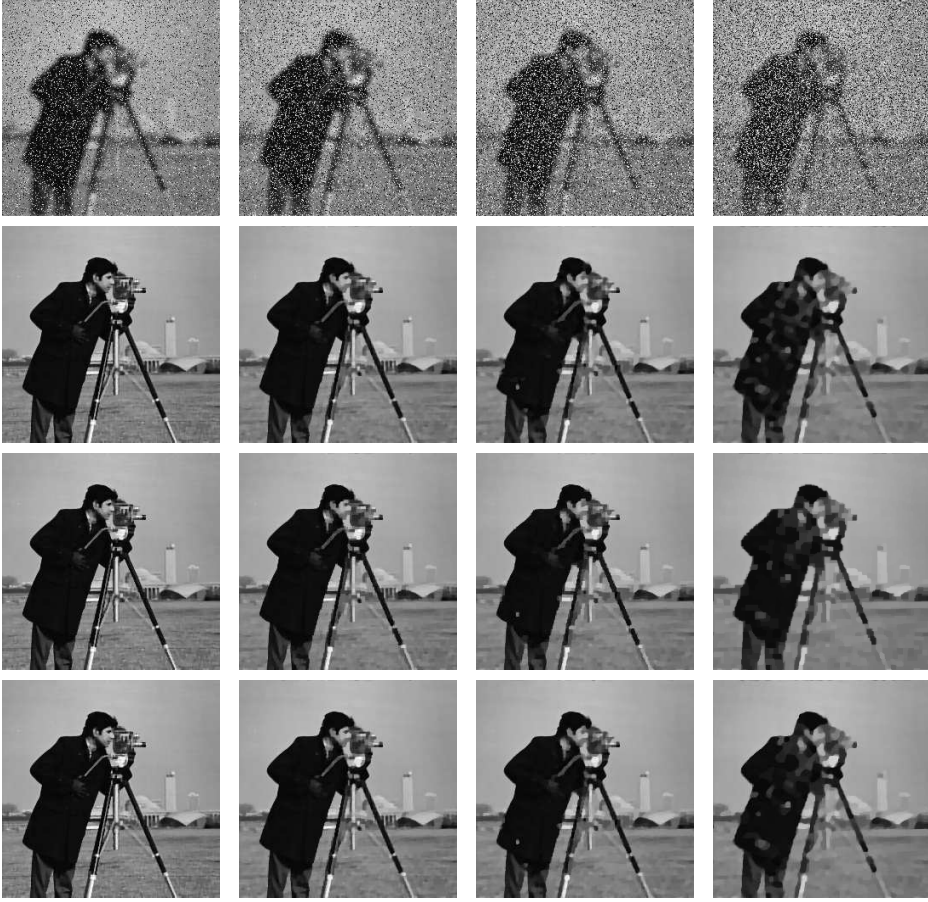
Fig. 5.2. *One-phase methods for restoration of the corrupted Cameraman images. The first row is the images corrupted by blur and the random-valued noise with noise levels 20%, 30%, 40% and 50% respectively. The rest rows from top to bottom give the images recovered by FTVd, ALM and proposed pdTV1.*

resulting SNRs of the FTVd algorithm and the proposed pdTV1 algorithm are comparable, and the proposed pdTV1 algorithm is much faster than the FTVd algorithm. In addition, the computational time by the proposed pdTV1 algorithm is comparable to the fastest algorithm ALM.

When this paper was nearly finished, we got to know that Chan et al. [18] proposed an algorithm for box-constrained TV-l^1 like one-phase model for image deblurring under impulse noise in their recently accepted paper. The model considered by Chan et al. [18] is:

$$\min_{0 \leq u \leq 255} \sum_{i,j} \sqrt{(\partial_x u_{ij})^2 + (\partial_y u_{ij})^2 + \beta} + \sum_{i,j} \sqrt{\left((Au)_{ij} - g_{ij}\right)^2 + \gamma}, \qquad (5.1)$$

where $\beta > 0, \gamma > 0$. When handling the box constraints, Chan et al. introduce constants $\varepsilon > 0$ to avoid possible zero denominators. Obviously, the values of these parameters have much impact on the performance of the algorithm, and need to be carefully chosen. In their algorithm, they also employ a line search which takes much computational cost. As suggested in [18], although Chan et al. obtained a sightly better PSNR gains compared with FTVd

Fig. 5.3. Two-phase methods for restoration of image Cameraman corrupted by blur and salt-and-pepper noise with noise levels 30%, 40%, 50% and 60% respectively. From top row to bottom row: filtered image, results recovered by Cai2008, Cai2010, proposed pdTV2 and pdNLTV2 method.

algorithm, their algorithm is much slower. However, our algorithm is much faster than FTVd algorithm, and these constants in (5.1) are not necessary in our algorithm.

5.2. Two-phase method

Here, we compare the proposed two-phase methods pdTV2 and pdNLTV2 with the algorithms Cai2008, Cai2010.

First, we give the experiments on the corrupted images used in the above subsection. The parameter η for the smooth regularization in algorithm Cai2010 is set to be $1/255^2$. There are several parameters in Cai2008, and it is not easy to fix them. We use the code provided by the author, and scale the intensity values of the corrupted images to $[0, 255]$, then we carefully select the parameters values according to the suggestion in [10]. We fix $\eta = 0.0001$, and the
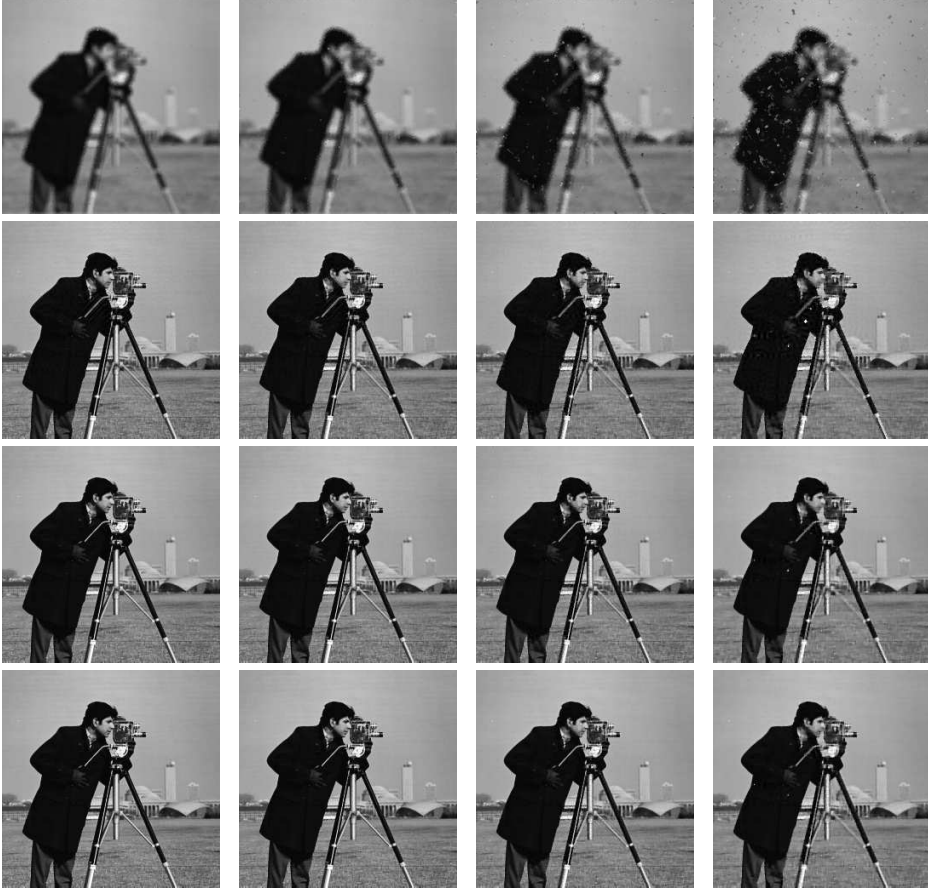
Fig. 5.4. Two-phase methods for restoration of the Cameraman image corrupted by blur and random-valued noise with noise levels 20%, 30%, 40% and 50% respectively. From top row to bottom row: filtered image results recovered by Cai2008, Cai2010 and pdNLTV2method.

other parameters $(\alpha, \beta, \epsilon)$ are given below.

For the salt-and-pepper noise with noise levels 30%, 40%, 50%, 60%: the parameters in Cai2008 are set to be $(2 \times 10^{-6}, 2 \times 10^{-6}, 0.001)$, $(2 \times 10^{-6}, 2 \times 10^{-6}, 0.001)$, $(5 \times 10^{-6}, 5 \times 10^{-6}, 0.001)$, $(5 \times 10^{-6}, 5 \times 10^{-6}, 0.0005)$ respectively; the regularization parameter β in Cai2010 is set to be $1/5000$; then the parameter λ in the proposed pdTV2 and pdNLTV2 algorithms is set to be $1/\beta$; the time step in the proposed pdTV2 and pdNLTV2 algorithms is set to be $t_u = 0.4/\lambda$; for the algorithm pdNLTV2, we set $h = 0.05$, and the number of neighbors be $(6+0)$ (the notation $(n_1 + n_2)$ means that the similar neighborhoods contain n_1 searched best and n_2 nearest neighborhoods).

For the random-valued noise with noise levels 20%, 30%, 40%, 50%: the parameters in Cai2008 are set to be $(2 \times 10^{-4}, 2 \times 10^{-4}, 0.001)$, $(4 \times 10^{-4}, 4 \times 10^{-4}, 0.001)$, $(7 \times 10^{-4}, 7 \times 10^{-4}, 0.001)$, $(0.001, 0.001, 0.0005)$ respectively; the regularization parameter β in Cai2010 is set to be $1/500$, $1/400$, $1/250$, $1/100$; then the parameter λ in the proposed pdTV2 and pdNLTV2 algorithms is set to be $1/2\beta$; The time step in the proposed pdTV2 and pdNLTV2 model is set to be $t_u = 0.04/\lambda$. For the pdNLTV2, we set $h = 0.01$, and the number of neighbors to be $(6+0)$ for first two images, $(4+4)$ for third image, and $(2+4)$ for the last one.

Fig. 5.5. Two-phase method for the restoration of the Cameraman image corrupted by blur and the salt-and-pepper noise with noise level 90%. From left to right: the corrupted image, the filtered image; the images recovered by Cai2008 (SNR=11.59dB, times=145.5s), Cai2010 (SNR=12.21dB, times=212.3s), proposed pdTV2 (SNR=12.39dB, times=28.8s) and pdNLTV2 (SNR=12.41dB, times=144.5s).

Table 5.2: SNR (dB) and computational times (in seconds) for the two-phase methods for the corrupted Cameraman image.

	salt-and-pepper				random-valued			
	30%	40%	50%	60%	20%	30%	40%	50%
Cai2008	20.92	19.50	18.11	16.52	21.02	19.24	17.21	14.86
	(276.6s)	(293.9s)	(268.0s)	(255.7s)	(416.3s)	(426.6s)	(470.0s)	(573.2s)
Cai2010	24.56	22.40	20.54	18.61	24.66	21.85	19.48	16.41
	(211.4s)	(216.8s)	(211.6s)	(216.7s)	(288.4s)	(315.4s)	(336.8s)	(395.0s)
pdTV2	25.67	23.62	21.55	19.27	24.97	22.09	19.53	16.43
	(61.2s)	(60.8s)	(62.0s)	(61.4s)	(52.1s)	(48.1s)	(42.3s)	(33.4s)
pdNLTV2	26.37	23.87	21.72	19.52	25.50	22.18	19.70	16.70
	(133.3s)	(146.6s)	(189.7s)	(132.9s)	(215.1s)	(138.3s)	(101.1s)	(56.2s)

Fig. 5.3 and Fig. 5.4 give the restored images. The filtered images obtained from applying AMF or ACWMF to the corrupted images are shown in the first row in each Figure respectively. It is obviously observed that the random-valued noise is more difficult to remove than the salt-and-pepper noise. Table 5.2 illustrate the SNR and computational times of the three methods. Clearly, the proposed pdTV2 is the fastest one. The proposed pdNLTV2 gets the best restored results, and the proposed two algorithms are both faster than the algorithms Cai2008 and Cai2010.

Next, we give experiments on the corrupted images with high level noise: 90% of the salt-and-pepper noise we set $(1 \times 10^{-5}, 1 \times 10^{-5}, 1 \times 10^{-4})$ for Cai2008, $\beta = 5000$ for Cai2010, $\lambda = 1/\beta, t_u = 5/\lambda$ for pdTV2, and $h = 0.05, \lambda = 1/\beta, t_u = 2.5/\lambda$ for pdNLTV2. Fig. 5.5 give the results. We can observe that the two-phase algorithms can handle high noise levels of the salt-and-pepper noise, and for the corrupted image, the one-phase algorithms cannot yield meaningful results. Although using the filtered image which has many errors to compute the weights, the proposed pdNLTV2 algorithm achieve highest restored quality.

Fig. 5.6. Original images. From left to right: Barbara, Boat, Couple, Man.

Table 5.3: SNR (dB) and computational times (in seconds) for various methods for other images blurred and corrupted by the salt-and-pepper noise with noise level 50%.

Images	One-phase method			Two-phase method			
	FTVd	ALM	pdTV1	Cai2008	Cai2010	pdTV2	pdNLTV2
Barbara	10.70	10.47	10.69	13.97	14.13	13.97	14.02
	(76.1s)	(18.5s)	(43.1s)	(1508.6s)	(1056.3s)	(612.0s)	(715.8s)
Boat	12.93	12.39	12.93	19.02	20.60	20.76	21.14
	(75.8s)	(19.1s)	(41.1s)	1286.3	(808.7s)	(403.1s)	(444.1s)
Couple	12.24	11.84	12.24	18.77	20.10	20.35	20.69
	(75.0s)	(18.0s)	(42.6s)	(1306.5)	(819.6s)	(435.2s)	(497.5s)
Man	14.40	13.77	14.40	19.61	20.93	21.20	21.50
	(76.9s)	(17.9s)	(47.4s)	(1613.9s)	(972.0s)	(447.5s)	(546.5s)
Average	12.57	12.11	12.57	18.52	19.47	19.58	19.84
	(76.0s)	(18.4s)	(43.6s)	(1364.3s)	(848.3s)	(456.0s)	(530.7s)

5.3. Experiments on Other Images

Now we give some results for the other 512×512 gray images (shown in Fig. 5.6) which are blurred and corrupted by the salt-and-pepper noise with noise level 50% or by the random-valued noise with noise level 40%. We set the parameters the same as the previous experiments on the corrupted image with the same noise level except for pdTV1, we set $t_u = 0.03/\lambda$ or $0.04/\lambda$ when dealing with the two different kinds of noise respectively; for pdTV2, we set $t_u = 0.2/\lambda$; for pdNLTV2, we set $t_u = 0.4/\lambda, h = 0.1$ and the number of the neighbors be $(2+4)$ for the salt-and-pepper noise, $t_u = 0.01/\lambda, h = 0.05$ and the number of the neighbors be $(4+4)$ for the random-valued noise. Tables 5.3 and 5.4 illustrate the SNR and computational times of various methods, and the proposed methods also exhibit good performance.

We do not give the results obtained from applying the algorithm pdTV2 to image deblurring and random-valued noise removal, because in this case, the algorithm pdNLTV2 is much faster than the algorithm Cai2010 and get better results. Although the algorithm pdTV2 is fastest (the average times=299.0s), the resulting average SNR is 18.49dB which is slightly lower than that obtained by the algorithm Cai2010.

5.4. About the convergence of the algorithms

Since the two-phase methods: Cai2008 and Cai2010, use preconditioned conjugate method to solve the corresponding inner linear systems. Thus it's not possible to show their convergence w.r.t. iteration. Here, we just give the comparison of the convergence of one-phase methods: FTVd, ALM, pdTV1. Fig. 5.7 gives one example. We can observe that the convergence rate

Table 5.4: SNR (dB) and computational times (in seconds) for various methods for other images blurred and corrupted by the random-valued noise with noise level 40%.

Images	One-phase method			Two-phase method		
	FTVd	ALM	pdTV1	Cai2008	Cai2010	pdNLTV2
Barbara	10.78	10.58	10.78	12.61	13.28	13.40
	(70.0s)	(16.4s)	(41.0s)	(1921.0s)	(1538.4s)	(628.4s)
Boat	13.26	12.74	13.30	18.72	19.82	20.00
	(70.9s)	(16.9s)	(39.5s)	(1882.2s)	(1208.9s)	(524.6s)
Couple	12.54	12.13	12.54	18.08	19.24	19.36
	(70.2s)	(16.2s)	(39.3s)	(1979.8s)	(808.7s)	(549.9s)
Man	14.24	13.77	14.32	18.96	19.81	19.94
	(73.5s)	(15.2s)	(43.4s)	(2507.5s)	(1635.7s)	(617.1s)
Average	12.71	12.31	12.74	17.83	18.66	18.76
	(71.2s)	(16.2s)	(40.8s)	(2047.5s)	(1270.6s)	(561.5s)

of pdTV1 is between ALM and FTVd. However, pdTV1 achieves highest SNR results.

6. Conclusion

In this paper, we present some effective and efficient algorithms for restoration of blurred images with impulse noise via box-constrained TV-type l^1 models. Both one-phase and two-phase methods are designed. And with the noise candidates information, the two-phase methods can yield much better results than the one-phase method, and can handle much higher impulse
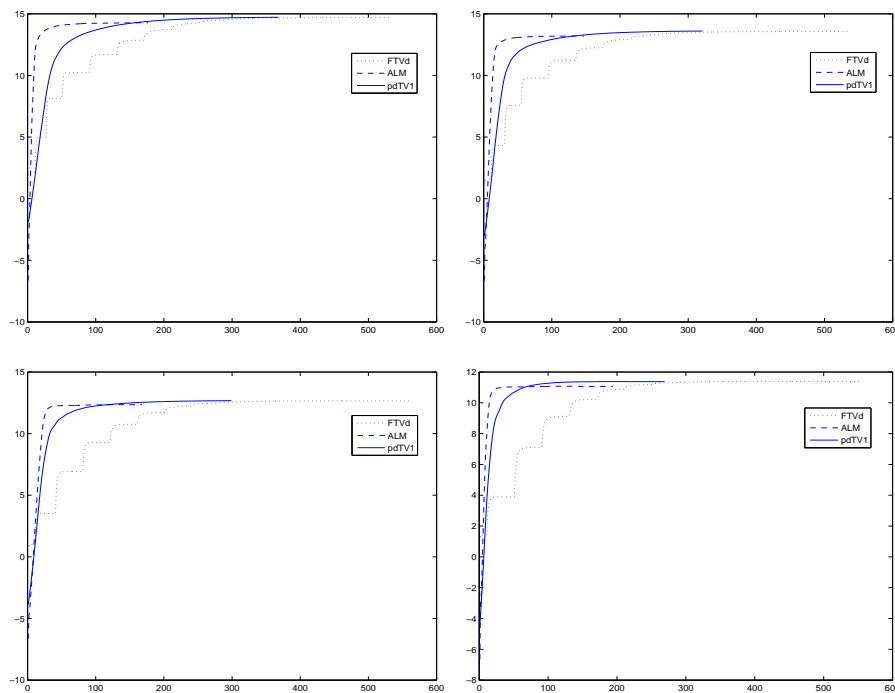

Fig. 5.7. From top to bottom and left to right: SNR gain vs. number of iterations of the Cameraman corrupted by blur and salt-and-pepper noise with noise levels 30%, 40%, 50%, 60% respectively.

noise level. By combining the nonlocal TV regularization, the algorithm can achieve much higher image restoration quality. However, since the selected neighbors and its weights in the nonlocal TV regularization play an important role, one should carefully select the suitable parameter values which are dependent on the images and the noise levels. As a matter of fact, these factors are all attributed to how to conveniently and effectively compute the similarity of the patches in the given image. In the future work, we will explore this important topic for analysis and for other image processing applications. The adaptive choice of the step-size t_d, t_u is also extremely interesting.

References

[1] H. Bahouri, J. Chemin, R. Danchin, Fourier Analysis and Nonlinear Partial Differential Equations, Springer, 2011.

[2] L. Bar, N. Sochen, N. Kiryati, Image deblurring in the presence of salt-and-pepper noise, *in Proc. 5th Int. Conf. Scale Space and PDE Methods in Computer Vision*, (2005), 107-118.

[3] L. Bar, N. Sochen, N. Kiryati, Image deblurring in the presence of impulsive noise, *Int. J. Comput. Vis.*, **70**:3 (2006), 279-298.

[4] L. Bar, N. Sochen, N. Kiryati, Deblurring of color images corrupted by salt-and-pepper noise, *IEEE Trans. Image Process.*, **16**:4 (2007), 1101-1111.

[5] S. Boyd, L. Vandenberghe, *Convex Optimization*, 91, Cambridge University Press, Cambridge, 2004.

[6] X. Bresson, A short note for nonlocal tv minimization, *Technical report*, 2009.

[7] D. Brownrigg, The weighted median filter, *Commun. ACM.*, **27**:8 (1984), 807-818.

[8] A. Buades, B. Coll, J.M. Morel, A review of image denoising algorithms, with a new one, *Multiscale Model. Simul.*, **4**:2 (2005), 490-530.

[9] A. Buades, B. Coll, J.M. Morel, Nonlocal Image and Movie Denoising, *Int. J. Comput. Vis.*, **76**:2 (2008), 123-139.

[10] J. Cai, R. Chan, M. Nikolova, Two-phase approach for deblurring images corrupted by impulse plus gaussian noise, *Inverse Problems Imag.*, **2**:2 (2008), 187-204.

[11] J. Cai, R. Chan, M. Nikolova, Fast two-phase image deblurring under impulse noise, *J. Math. Imag. Vis.*, **36**:1 (2010), 46-53.

[12] T. Chen, H.R. Wu, Space variant median filters for the restoration of the impulse noise corrupted images, *IEEE Trans. Circuits Syst. II*, **48**:8 (2001), 784-789.

[13] A. Chambolle, An algorithm for total variation minimization and applications, *J. Math. Imag. Vis.*, **20**:1-2 (2004), 89-97.

[14] A. Chambolle, T. Pock, A First-Order Primal-Dual Algorithm for Convex Problems with Applications to Imaging, *J. Math. Imaging Vis.*, **40**:1 (2011), 120-145.

[15] R. Chan, Y. Dong, M. Hintermüller, An efficient two-phase l^1-TV method for restoring blurred images with impulse noise, *IEEE Trans. Image Process.*, **19**:7 (2010), 1731-1739.

[16] A. Effros, T. Leung, Texture synthesis by non-parametric sampling, *in Proc. 7th IEEE Int. Conf. Comput. Vis.*, 1999, pp.1033-1038.

[17] T. Chan, G. Golub, P. Mulet, A nonlinear primal-dual method for total variation-based image restoration, *J. SIAM J. Sci. Comp.*, **20**:6 (1999), 1964-1977.

[18] R. Chan, J. Ma, A multiplicative iterative algorithm for box-constrained penalized likelihood image restoration, *IEEE trans. Image Process.*, In press.

[19] P. Combettes, V. Wajs, Signal recovery by proximal forward backward splitting, *Multiscale Model. Simul.*, **4**:4 (2005), 1168-1200.

[20] B. Dong, H. Ji, J Li, Z. Shen, Y. Xu, Wavelet frame based blind image inpainting, *Appl. Comput. Harmon. A.*, **32**:2 (2012),268-279.

[21] Y. Dong, M. Hintermüler, M. Neri, An Efficient Primal-Dual Method for L^1TV Image Restoration, *SIAM J. Imag. Sci.*, **2**:4 (2009), 1168-1189.

[22] S. Geman, D. Geman, Stochastic relaxation, Gibbs distributions, and the Bayesian restoration of images, *IEEE Trans. Pattern Anal.Mach. Intell.*, **6**:6 (1984), 721-741.

[23] X. Guo, F. Li, M.K. Ng, A Fast l^1-TV Algorithm for Image Restoration, *SIAM J. Sci. Comput.*, **31**:3 (2009), 2322-2341.

[24] G. Gilboa, S. Osher, Nonlocal operators with applications to image processing, *Multiscale Model. Simul.*, **7**:3 (2008), 1005-1028.

[25] T. Goldstein, S. Osher, The split Bregman algorithm for L1 regularized problems, *SIAM J. Imag. Sci.*, **2**:2 (2009), 323-343.

[26] W. Hager, B. Mair, H. Zhang, An Affine-scaling interior-point CBB method for box-constrained optimization, *Mathematical Programming*, **119** (2009), 1-32.

[27] J. Hiriart-Urruty, C. Lemarechal, *Convex analysis and minimization algorithms I*, Springer-Verlag, Berlin Herdelberg, 1993.

[28] H. Hwang, R. Haddad, Adaptive median filters: new algorithms and results, *IEEE Trans. Image Process.*, **4**:4 (1995), 499-502.

[29] M. Jung, X. Bresson, T.F. Chan, L.A. Vese, Nonlocal Mumford-Shah Regularizers for Color Image Restoration, *IEEE Trans. Image Process.*, **20**:6 (2011), 1583-1598.

[30] M. Jung, L.A. Vese, Nonlocal variational image deblurring models in the presence of Gaussian or impulse noise, *in Proc. 5th Int. Conf. Scale Space and Variational Methods in Computer Vision*, 1999, pp.402–413.

[31] D. Kim, S. Sra, I. Dhillon, Tackling box-constrained optimization via a new projected quasi-newton approach, *SIAM J. Sci. Comput.*, **32**:6 (2010), 3548-3563.

[32] S. Ko, Y. Lee, Center weighted median filters and their applications to image enhancement, *IEEE Trans. Circuits Syst.*, **38**:9 (1991), 984-993.

[33] J. Moreau, Fonctions convexes duales et points proximaux dans un espace hilbertien, *C.R. Acad. Sci. Paris Ser. A Math.*, **255**(1962), 1897-2899.

[34] J. Moreau, Proximite et dualite dans un espace hilbertien, *Bull. Soc. Math. France.*, **93**(1965), 273-299.

[35] B. Morini, M. Porcelli, R. Chan, A Reduced Newton Method for Constrained Linear Least-Squares Problem, *Journal of Computational and Applied Mathematics*, **233** (2010), 2200-2212.

[36] D. Mumford, J. Shah, Optimal approximations by piecewise smooth functions and associated variational problems, *CPAM*, **42**:5 (1989), 577-585.

[37] M. Nikolova, Minimizers of cost-functions involving nonsmooth data-fidelity terms. Application to the processing of outliers, *SIAM J. Numer. Anal.*, **40**:3 (2002), 965-994.

[38] M. Nikolova, A variational approach to remove outliers and impulse noise, *J. Math. Imag. Vis.*, **20**:1-2 (2004), 99-120.

[39] W. Pratt, Median filtering, *Tech. Rep.*, Image Proc. Inst., Univ. Southern California, Los Angeles, 1975.

[40] L. Rudin, S. Osher, E. Fatemi, Nonlinear total variation based noise removal algorithms, *Physica D*, **60**(1992), 259-268.

[41] Y. Wang, S. Ma, Projected Barzilai-Borwein method for large-scale nonnegative image restoration, *Inverse Problems in Science and Engineering*, **15** (2007), 559-583.

[42] W. Wang, M.K. Ng, On algorithms for automatic deblurring from a single image, *Journal of*

Computational Mathematics, **30**:1 (2012), 80-100.

[43] Y. Wang, J. Yang, W. Yin, and Y. Zhang, A new alternating minimization algorithm for total variation image reconstruction, *SIAM J. Imaging. Sci.*, **1**:3 (2008), 248272.

[44] M. Werlberger, T. Pock, M. Unger, H. Bischof, Optical flow guided TV-l^1 video interpolation and restoration, *In EMMCVPR*, 2011, pp.273-286.

[45] C. Wu, J. Zhang, X. Tai, Augmented lagrangian method for total variation restoration with non-quadratic fidelity, *Inverse Problems Imag.*, **5**:1 (2011), 237-261.

[46] Y. Xiao, T. Zeng, J. Yu, M. Ng, Restoration of images corrupted by mixed Gaussian-impulse noise via $l^1 - l^0$ minimization, *Pattern Recognition*, **44**:8 (2011), 1708-1720.

[47] F. Yang, K. Chen, B. Yu, Homotopy curve tracking for total varization image restoration, *Journal of Computational Mathematics*, **30**:2 (2012), 177-196.

[48] J. Yang, Y. Zhang, W. Yin, An efficient TVL1 algorithm for deblurring multichannel images corrupted by impulsive noise, *SIAM J. Sci. Comput.*, **31**:4 (2009), 2842-2865.

[49] X. Zhang, M. Burger, X. Bresson, S. Osher, Bregmanized Nonlocal Regularization for Deconvolution and Sparse Reconstruction, *SIAM J. Imag. Sci.*, **3**:3 ,(2010) 253–276.

[50] M. Zhu, T. Chan, An efficient primal-dual hybrid gradient algorithm for total variation image restoration, *UCLA CAM Report 08-34*, 2007.